

MiLAAP : Mobile Link Allocation via Attention-based Prediction

Yung-Fu Chen
The Ohio State University
USA
chen.6655@osu.edu

Anish Arora
The Ohio State University
USA
arora.9@osu.edu

ABSTRACT

Channel hopping communication systems must adapt to interference changes in the wireless network and to node mobility for maintaining their throughput efficiency. Optimal channel hopping scheduling requires up-to-date network state information (i.e., of channel occupancy) to select non-overlapping channels for network links in interference regions. However, state sharing among nodes introduces significant communication overhead, especially as network size or node mobility scale, thereby decreasing throughput efficiency of already capacity-limited networks. In this paper, we eschew state sharing while adapting the channel hopping schedule based on a learning-based channel occupancy prediction. We propose the MiLAAP attention-based prediction framework for machine learning models of spectral, spatial, and temporal dependencies among network nodes. MiLAAP uses a self-attention mechanism that lets each node capture the temporospectral channel hopping pattern in its interference region and accordingly predict the channel occupancy state within that region. Notably, the prediction relies only on locally and passively observed channel activities, and thus introduces no communication overhead. To deal with node mobility, MiLAAP also uses a multi-head self-attention mechanism that lets each node locally capture the spatiotemporal dependencies on other network nodes that can interfere with it and accordingly predict the motion trajectory of those nodes. Detecting nodes that enter or move outside the interference region is used to further improve the prediction accuracy of channel occupancy. We show that for dynamic networks that use local channel hopping sequences to support relatively long-lived flow traffics, the channel state prediction accuracy of MiLAAP is remarkably $\sim 100\%$ across different node mobility patterns and it achieves zero-shot generalizability across different periods of channel hopping sequences.

KEYWORDS

Machine learning, self-attention, sequence to sequence model, channel hopping, channel prediction, mobility detection, interference avoidance

1 INTRODUCTION

Channel hopping (aka frequency hopping) has been widely adopted in wireless communication systems to mitigate interference as well as resist active jamming and passive eavesdropping attacks. It combines a slotted time schedule for multi-channel medium access with a channel hopping mechanism, to effectively avoid collisions in concurrent transmissions. Typically, the channel hopping mechanism for a communication link uses a pre-defined channel hopping sequence repeatedly to assign the channel to be used for each time slot. Minimization of interference is achieved by properly scheduling the channel hopping sequence among the active communication links.

As demands for network applications grow in contexts with wireless environment changes and node mobility, channel hopping communication systems are needing to evolve to deal with network dynamics. This is the case, for example, in low-rate and low-power communication systems, such as the Industrial Internet of Things (IIoT) [16] and Edge Internet of Things [19], where channel hopping has gained significant adoption but is inadequately solved for interference and mobility dynamics. IIoT connects industrial equipment, sensors, and devices in industrial settings through the Internet to optimize processes and improve efficiency, productivity, and decision-making through real-time observation. Edge IoT focuses on optimizing local data processing and communication, reducing latency, and improving overall system efficiency. Time Slotted Channel Hopping (TSCH), a medium access control (MAC) protocol included in the IEEE 802.15.4e standard [1], is often employed in both industrial and edge IoT. TSCH-based networks typically share a globally fixed channel sequence and rely on a channel offset schedule to assign nodes different indexes to the global channel hopping sequence to avoid interference. The IEEE 802.15.4 standard leaves the choice of channel hopping sequence scheduler to the protocol implementer. Scheduling may be centralized or distributed [17]. TSCH does not provide a specific mechanism to manage node mobility. Although a few mobility-aware scheduling protocols have been proposed in TSCH-based networks [4, 18, 20], for dynamic networks efficient scheduler designs for TSCH networks are still lacking.

Similarly, channel hopping has been adopted in long-range satellite communication systems. Satellite networks, such as Intelsat [3], Inmarsat [2], and Eutelsat [10], utilize low Earth orbit (LEO) satellites to offer lower latency and higher bandwidth, and geostationary Earth orbit (GEO) satellites to provide broad coverage. Channel hopping is applied to communication between LEO and GEO satellites, where LEO satellites can transmit simultaneously to a GEO satellite. Since rapid change in environmental conditions causes interference across channels to alter materially, dynamic channel hopping [5] addresses limitations of the static channel hopping approach to improve communication resilience, security, interference mitigation, and cost-effectiveness.

Machine learning for dynamic channel hopping. Dynamic channel hopping adapts the channel hopping sequence in response to changes in channel quality and interference conditions. Typically, this is accomplished through proactive spectrum sensing and message exchange with neighboring nodes to obtain these measures. However, frequent message exchange among nodes introduces significant communication overhead, thereby decreasing throughput efficiency, especially in large or more mobile wireless networks. Scaling the overhead of obtaining up-to-date network states in dynamic networks remains a challenging issue. In this paper, we consider the alternative of eschewing explicit network

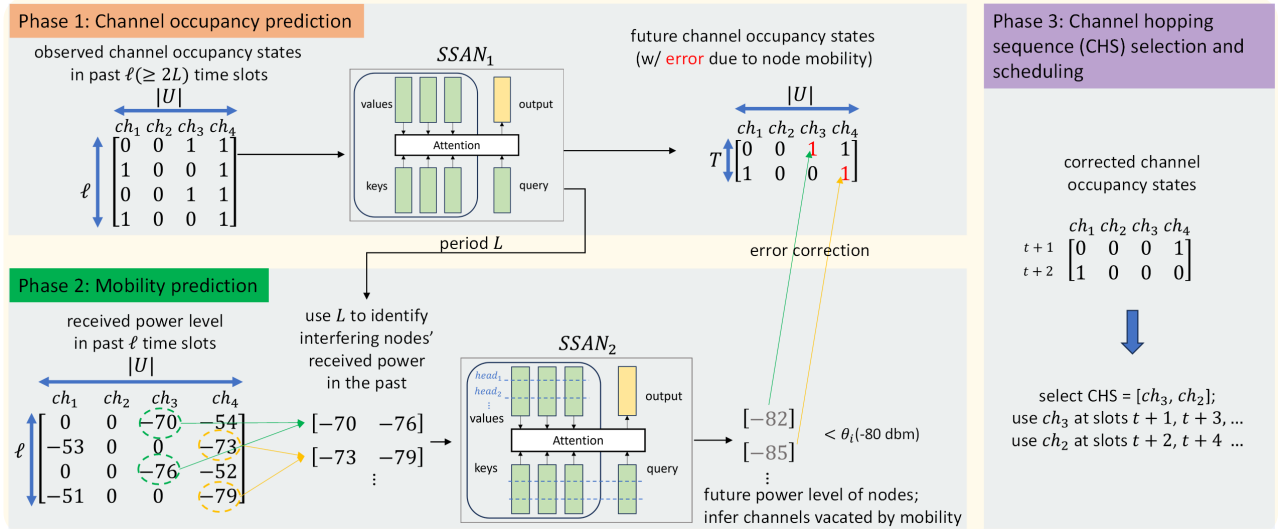


Figure 1: Illustration of the procedure for mobile link allocation in MiLAAP : Prediction of occupancy of the $|U|$ channels by a seq2seq attention network (Phase 1) identifies unoccupied channels that are used to select the node's new local channel hopping sequence of period L (Phase 3). As an intermediate step, prediction of received power level from other nodes by another seq2seq attention network (Phase 2) is used to detect entry or departure of nodes from the node's interference region and expedite the correction of predicted channel occupancy states

state sharing, with an alternative approach that predicts network states in the presence of network dynamics using machine learning.

Empirical studies have shown that it is possible to learn link correlations from information observed at the network nodes. The work in [12, 14] shows that channel hopping sequences can be predicted from historical spectrum data using long short-term memory (LSTM) and convolutional neural (CNN) networks. Other work has demonstrated the feasibility of reverse engineering the channel hopping sequence by eavesdropping on unencrypted packet headers transmitted over networks [8, 9]. However, these studies have not considered network dynamics, including node mobility or external interference, and their approach did not perform well in our preliminary experiments with dynamic networks.

The MiLAAP¹ approach. To address the above-mentioned issues, we formulate a problem of wireless network state prediction in the presence of dynamic interference and node mobility—more specifically, per node prediction of channel occupancy (CO) state. For each node, the prediction is used to adapt its channel hopping sequence when its channel occupancy state changes, by reassigning non-overlapping frequencies. We show that the prediction problem is solvable from historical data observed locally and passively in relatively broad contexts, e.g., where a channel hopping schedule per node is used for relatively-long lived flow traffics. Our MiLAAP solution thus introduces zero communication overhead for prediction.

The key objective in the MiLAAP approach is to rapidly capture temporal, spectral, and spatial dependencies between mobile nodes. The channel occupancy state at a node results from the superposition of the channel hopping sequences of all transmitters within the

interference range of the node. Its prediction therefore involves capturing temporospectral correlations. Moreover, since it changes as other nodes move in and out of the interference region of the node, predicting node mobility also to expedite its prediction is useful and involves capturing temporospatial correlations. MiLAAP accordingly solves the prediction problem in two phases, as depicted in Fig. 1: the first phase addresses the channel occupancy prediction problem by capturing the regular period of the superposed channel hopping sequences. The second phase addresses the mobility detection problem by predicting the received power level of neighboring nodes to infer whether nodes are moving out from the interference region of the node. The multi-head attention mechanism has been shown to have the ability to learn complex temporospectral and temporospatial dependencies [13, 15]. MiLAAP therefore adopts an attention-based seq2seq learning architecture [6, 22].

Contributions of the paper. We highlight three aspects of MiLAAP :

- (1) Its ML-based approach predicts channel occupancy states at each node using only locally and passively observed information. The prediction suffices for minimizing interference in the dynamic setting by locally adapting and scheduling channel hopping sequences. As no communication overhead is introduced in this process, it yields higher throughput efficiency for medium access scheduling as compared to MAC protocols relying on alternative proactive or reactive approaches for selecting unoccupied channels.
- (2) A single layer sequence masked self-attention network suffices for the first phase of MiLAAP to capture the temporospectral pattern in the superposed channel hopping sequences. When evaluated for static wireless networks, the

¹"Milaap" means coming together in unison in Hindi.

pre-trained model achieves ~100% accuracy and also generalizes to networks where different nodes can use channel hopping sequences of different periods.

- (3) Adding a multi-head masked self-attention layer for the second phase of MiLAAP suffices to capture temporospatial dependencies for predicting the trajectory of mobile nodes. The resulting pre-trained model allows MiLAAP to locally detect when nodes leave or enter the interference region of a node. This significantly expedites the responsiveness of the node’s update of its channel hopping sequence. When evaluated in mobile wireless networks, MiLAAP achieves ~100% accuracy again in its prediction of channel occupancy. We also show that learning is feasible for different node mobility patterns.

Organization. The rest of the paper is organized as follows. In Section 2, we discuss related prior work. In Sections 3 and 4, we formalize the two-phase prediction problem and then present our Attention-based seq2seq solution to capturing the spatial, temporal, and spectral dependencies. We present evaluation results in Section 5, and make concluding remarks in Section 6.

2 RELATED WORK

2.1 Time Slotted Channel Hopping (TSCH)

TSCH is a channel hopping MAC protocol incorporated in the IEEE 802.15.4e standard [1]. It inherits slotted time access from IEEE 802.15.4. To achieve reliable performance in the presence of interference and multipath fading, it leverages multi-channel communication and channel hopping based on a synchronized slotframe. Each slotframe is a collection of slots with a fixed length that repeats over time; every slot is long enough to transmit a data packet and receive an acknowledgment between a pair of nodes within some transmission radius.

Channel hopping in TSCH relies on channel offset schedules to avoid internal interference (and, in turn, communication collisions). The offset schedule is defined over a predefined sequence of channels, i.e., it is a globally shared sequence, instead of a randomly generated channel sequence. This is done primarily to reduce the overhead of channel synchronization. The communication channel to be used for transmission and reception over a link at a slot ASN follows the function CHS :

$$Channel(ASN) = CHS [(ASN + OF) \bmod L], \quad (1)$$

where ASN stands for the absolute slot number, OF is the channel offset of a communication link between two nodes, and L denotes the period of a channel hopping sequence. The idea is to assign a different OF to links that can potentially interfere. Several heuristics [11] have been proposed to maximize the end-to-end reliability and minimize the end-to-end delay in TSCH MAC protocols, either by centralized or by distributed scheduling of a node’s transmission time slots (time diversity) and the channel offset in Eq. 1 (frequency diversity).

2.2 Local Channel Hopping Sequences

Even though TSCH-based protocols have shown good performance in industrial environments with stable topologies and low traffic, their reliance on a globally shared channel sequence limits their

robustness to network dynamics. When L becomes small, the ability to avoid interference is negatively impacted. Furthermore, the use of a global channel hopping sequence inherently limits its resilience with respect to concurrent communications. The number of transmission links within an interference region must be at most L to avoid collision. If $L+1$ links exist within the interference region, there exist at least two links that will collide predictably. In this case, the achievable capacity is reduced by at least $\frac{1}{L}$, which is more than the expected reduction when scheduling with random channel sequences.

It has been demonstrated [7] that in an interference region with concurrent flows where $\#(available\ channels) \geq \#(active\ nodes) \geq \#(flows) > 1$, scheduling with fixed per-link channel hopping sequences achieves a performance that is competitive with scheduling with global or random channel hopping sequences. Selection of the local channel hopping sequences is achieved by active coordination among the active nodes in the interference region, yielding potentially different sequences for different nodes. To the best of our knowledge, previous work has not considered passive, local selection of the sequences. But it has motivated the feasibility of adapting the sequence when the interference changes. Since the local channel hopping sequence approach has been shown to outperform the throughput efficiency of global and random sequences, we will use it as the baseline for the comparative evaluation of our ML-based passive, local selection solution.

3 PROBLEM STATEMENT

The primary objective of mobile link allocation is to efficiently assign a limited network resource —communication channels— to mobile nodes in a way that minimizes the interference over all links active within each node’s interference region. Efficiency involves keeping the overhead of selecting channels and the schedules low. The objective can be achieved as follows: given an accurate channel occupancy state in each interference region of each node, minimize collisions by assigning non-overlapping channels for transmission, say by solving an instance of the graph coloring problem. We formalize the objective in terms of first accurately and efficiently predicting the channel occupancy state at each node and then choosing a local channel sequence at each node that minimizes interference.

3.1 System Model

The communication system uses slotted-time access, multi-channel communication, and channel hopping based on a synchronized slotframe. Each slotframe is a collection of slots with a fixed length that repeats over time; every slot is long enough to transmit a data packet and receive an acknowledgment via a link between a pair of nodes within some transmission radius. Each link corresponds to two nodes; without loss of generality, we let each link be assigned to use one channel at a given time slot.

3.1.1 Communication Model. A local channel hopping sequence CHS_i is associated with each node i . CHS_i determines the communication channel used by i to transmit at time slot t :

$$Channel_i(t) = CHS_i [t \bmod L], \quad (2)$$

where L is the period (or, equivalently, the length) of CHS_i . The channel hopping sequence may be different for different nodes.

Table 1: Notations for MiLAAP

Symbol	Meaning
U	set of all channels
L	period of a channel hopping sequence
i	node id
(i, j)	link id
$ch \in U$	channel id
t	time slot number
$\Phi(i)$	set of nodes in i 's interference region
CHS_i	channel hopping sequence for node i
r_T	radius of reliable transmission region
r_I	radius of interference region
r_S	radius of sensing region
$CO_t(i) \in [0, 1]^{ U }$	vector of monitored channel occupancy states in i 's interference region at time t
$CO_t(i, ch) \in [0, 1]$	ch 's channel occupancy state in i 's interference region at time t
$RP_t(i) \in \mathbb{R}^{ U }$	vector of received power level over channels observed at i at time t
$RP_t(i, ch) \in \mathbb{R}$	ch 's received power level at i at time t
θ_i	minimum received power level at i from j transmitting in i 's interference region

We assume a unit-disk interference model [21]. Let M be the number of active nodes that transmit traffic within an interference region. It is easy to see that L must be at least M to avoid interference within the region. For ease of presentation, let us assume that all nodes use a common, fixed L . In this case, the following thought-experiment provides intuition for the local predictability of the channel occupancy in the interference region of a node: Let all nodes transmit in each slot. Then the channel occupancy at node i will be the superposition of the channel hopping sequences of all nodes in the interference region of i . This channel occupancy will have a period of L and can hence be predicted by i by observing the channel occupancy over at least $2L$ time slots.²

To observe channel occupancy states in a time slot t , $CO_t(i)$, node i samples the medium in the channels to determine whether or not some signal is present. (The samples could be based on typical radio mechanisms such as Clear Channel Assessment [CCA], Received Signal Strength Indicator [RSSI], Channel State Indicator [CSI], or Signal to Noise Ratio [SNR].) For simplicity, we assume that all channels in U can be sampled in any given time slot.³

3.1.2 Traffic Model. We assume the network supports traffic flows whose arrival and departure rate is not too fast. In other words, self-interference in static networks changes when a flow arrives or departs but, by assumption, the duration between changes is larger than the duration of channel occupancy prediction and channel hopping sequence update.

²The use of different L in an interference region is likewise feasible: in the same thought experiment, the predictor can capture the period by observing time slots over at least twice the least common multiple of the different L used by the nodes.

³In practice, the sampling can be done in batches of size K_i , $K_i \geq 1$, collected every U/K_i timeslots, and the number of time slots to be observed for prediction can be scaled accordingly.

3.1.3 Mobility Model. Each network node can move within the network area, controlling its velocity and direction independently and unbeknownst to other nodes. We assume network mobility entails arrival and departure rates from interference regions which are not too fast. Thus again, by assumption, the duration between changes in node arrival or departure is larger than the duration of CO prediction and CHS update.

3.2 Predicting Channel Occupancy in Static and Mobile Networks

To maximize prediction accuracy, i learns both long-term temporospectral dependencies and dynamical temporospatial dependencies. For the former, i learns a model that predicts future channel occupancy states (i.e., the period of channel hopping sequences) associated with active nodes within i 's interference region. For the latter, i tracks node mobility via the received power level from nodes j in its interference region and accordingly predicts when nodes enter or leave its interference region.⁴ Fig. 2 illustrates an example of how channel occupancy in the interference region of a node i exhibits cyclic behavior—during time $t + 1$ and $t + 6$ where the set of nodes in the region remains unchanged. It also shows how the channel occupancy changes as nodes $-j_2$ at time $t + 1$ —move in and $-j_1$ at time $t + 7$ —move out of the interference region of node i . Predicting node mobility helps to infer when active nodes leave or enter the interference region of a node.

3.2.1 Channel Occupancy Prediction. Let $CO_t = [o_{ch} | ch \in U]$ denote the vector of channel occupancy states observed by node i at time slot t , where $o_{ch} \in \{0, 1\}$ is 1 if channel ch is occupied at t , and U is the set of all channels. We formulate the learning problem for channel occupancy prediction as follows:

Given ℓ historical vectors of channel occupancy states, $CO_{t-\ell+1}, \dots, CO_t$, observed by node i within its interference region, learn a channel occupancy prediction model is learned to predict T future vectors of channel occupancy states $CO_{t+1}, \dots, CO_{t+T}$.

3.2.2 Received Power Level Prediction for Mobility Detection. To enable inference of the time slot at which an active node is entering or moving out of i 's interference region, we formulate a learning problem for received power level prediction as follows:

Given ℓ historical states of received power level from node $j \in \Phi(i)$, $s_{t-\ell+1}, \dots, s_t$, observed by node i , learn a model at i that predicts the subsequent T states of j , s_{t+1}, \dots, s_{t+T} .

If the prediction of the power level received in transmissions from j drops below the threshold for interference detection, i can infer that j will have moved out of its interference regions. Conversely, if a power level above the threshold is observed afresh, i can infer that j has entered its interference region. These observations can be used to expedite update of the channel hopping sequence (and also the schedule of i .)

⁴Recall that the schedule for each node i can be determined based on the prediction that i makes for channel occupancy. The details of how the schedule of i is selected given the prediction, including how and when the channel hopping schedule is updated and how scheduling efficiency is optimized, are outside the scope of our presentation. Here, we focus on defining the prediction sub-problems.

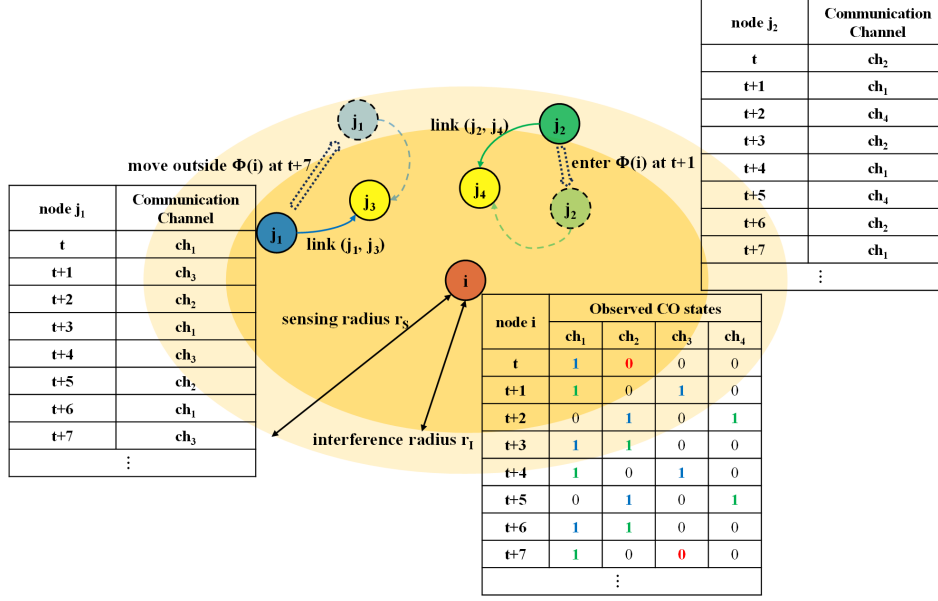


Figure 2: Example of channel occupancy (CO) vectors observed by node i in a mobile network with $L = 3$. The channel hopping sequences of nodes j_1 and j_2 are $CHS_{j_1} = ch_1; ch_3; ch_2$ and $CHS_{j_2} = ch_2; ch_1; ch_4$. From time $t + 1$, when both j_1 and j_2 are in i 's interference, the CO vector repeats every L time slots until $t + 7$, when j_1 leaves the region. i can detect the entry of j_2 into the region at $t + 1$ from CO_t and CO_{t+1} and predict the leave of j_1 at $t + 7$ from the received power trajectory in preceding slots

4 MiLAAP SOLUTION FRAMEWORK

As depicted in Fig. 1, the MiLAAP framework consists of two sequence-to-sequence attention networks, $SSAN_1$ and $SSAN_2$, that solve the prediction problems in § 3.2.1 and § 3.2.2 respectively. $SSAN_1$ uses a single masking self-attention layer to capture the common period (or the least common multiple period) of the channel hopping sequences of nodes in the interference region to predict future channel occupancy vectors; $SSAN_2$ adopts a single multi-head masking self-attention layer to predict future received power levels from the nodes in the sensing region.

4.1 First-Phase Prediction of CO Vectors and Capture of CHS Period

Given the assumption that all nodes in the interference region of node i in a static network have CHSes of a common period L , if all of them transmit continually, it follows that $CO_t(i)$ is identical to $CO_{t+kL}(i)$, $k \in \mathbb{N}$. The functionality of $SSAN_1$, which includes capturing L and using L to predict the subsequent CO vectors, is specified as follows. The input to $SSAN_1$ is $X \in [0, 1]^{\ell \times |U|}$, consisting of ℓ historical vectors of channel occupancy states observed by i , $CO_{t-\ell+1}(i), \dots, CO_t(i)$. $SSAN_1$ computes the queries (M_Q), keys (M_K), and values (M_V) on X as:

$$\begin{aligned} M_Q &:= XW_Q \\ M_K &:= XW_K \\ M_V &:= XW_V, \end{aligned} \quad (3)$$

where $W_Q, W_K, W_V \in \mathbb{R}^{|U| \times |U|}$ are the learned linear mappings for the queries, keys, and values, respectively. The mappings are performed by the feedforward neural networks.

The calculation scheme of $SSAN_1$ is shown as follows:

$$\begin{aligned} scores &:= \text{AttentionScore}(M_Q, M_K) \\ weights &:= \text{Softmax}(scores) \\ period &:= \text{CalculatePeriod}(weights) \\ M_{shifted} &:= \text{MatrixShift}(M_V, period) \\ Y &:= \text{BinOutput}(M_{shifted}W_O), \end{aligned} \quad (4)$$

where $W_O \in \mathbb{R}^{|U| \times |U|}$ is the learnable weight matrices for the output $Y \in [0, 1]^{|U|}$. The attention scores are calculated first and Softmax is used to normalize the scores to get a probability distribution (i.e., the attention weights). Then, we add a function, *CalculatePeriod*, that captures the common period of the input vectors based on the attention weights. Fig. 3 shows an example of an attention weight matrix computed for an input of 20 vectors with $L = 7$. The channel hopping pattern period of 7, where $CO_t = CO_{t+7}$, $t = 0, 1, \dots, 12$, is evidently modeled in the attention weights. The function captures the common period by determining the high weights (dark red cells) and then calculating the period (i.e., the distance between the high weights in each row) that appears most often. If the input length ℓ is not divisible by L , an offset is added for the following prediction. Lastly, *MatrixShift* operates to rollover the rows in M_V based on the offset ($\ell \% L$) so that $M_{shifted}$ can then be used for predicting the output Y , as follows:

$$\begin{aligned} offset &:= \ell \% L \\ M_{shifted}[i] &:= M_V[(i + offset) \% L], \quad i = 0..T - 1 \\ Y &:= \text{BinOutput}(M_{shifted}W_O) \end{aligned} \quad (5)$$

where function *BinOutput* rounds the elements below 0.5 in a matrix into 0s and those above 0.5 into 1s.

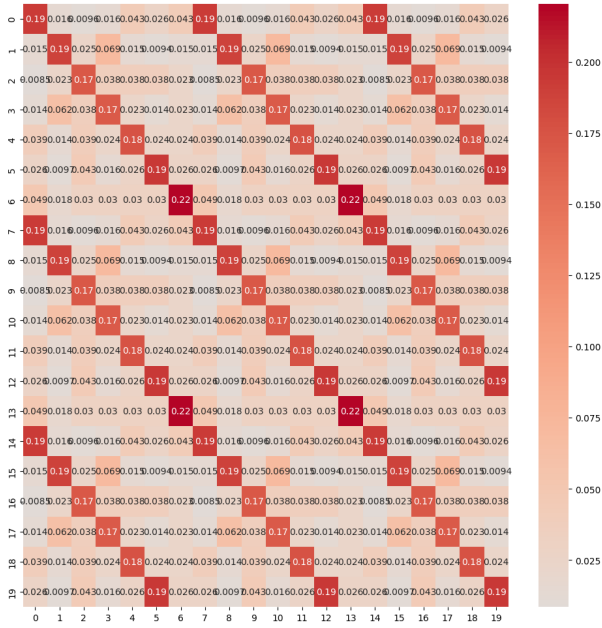


Figure 3: Example of attention weights for the channel occupancy vectors of length 20 and $L = 7$. There exists a pattern of period of 7 which can be used to predict the future channel occupancy vectors

4.2 Second-Phase Prediction of Received Power Levels

Let $RP_t(i) \in \mathbb{R}^{|U|}$ denote the vector of received power level of all channels observed by node i at time slot t . In addition to the $CO_{t-\ell+1}(i), \dots, CO_t(i)$ vectors monitored from $t - \ell + 1$ to t , node i also collects $RP_{t-\ell+1}(i), \dots, RP_t(i)$. Since the ID of node j transmitting over a monitored channel ch at time t can be unknown to node i , it suffices that i know that $\{RP_{t-kL}(ch, i) | k = 0 \dots \lfloor \frac{\ell}{L} \rfloor - 1\}$ can be associated with the same node using the L calculated in the first-phase prediction.⁵ Therefore, $\{RP_{t-kL}(ch, i) | k = 0 \dots \lfloor \frac{\ell}{L} \rfloor - 1\}$ can be used as the historical data sequence associated with some nodes to predict its future received power levels. $SSAN_2$ adopts a multi-head masking self-attention layer, in which each independent head has the opportunity to learn a different mobility pattern (e.g., a node coming into or vacating i 's interference region). The input to $SSAN_2$, X , is $\left[RP_{t-\lfloor \frac{\ell}{L} \rfloor L}(ch, i), RP_{t-\lfloor \frac{\ell}{L} \rfloor L}(ch, i), \dots, RP_t(ch, i) \right] \in \mathbb{R}^{\lfloor \frac{\ell}{L} \rfloor}$. $SSAN_2$ computes the queries (M_h^Q), keys (M_h^K), and values (M_h^V) for head h according to Eq. 3. The calculation scheme in $SSAN_2$ is shown as follows:

$$\begin{aligned}
 scores_h &:= \text{AttentionScore}(M_h^Q, M_h^K) \\
 M_h^W &:= \text{Softmax}(scores_h) \\
 M_h^V &:= \text{Concat}(M_1^W M_1^V, \dots, M_n^W M_n^V) \\
 Y &:= \text{BinOutput}(M_h^V M_h^W)
 \end{aligned} \tag{6}$$

⁵For the case where two nodes j_1 and j_2 use the same channel for communication at t , we assume the one with less distance to node i dominates the received power level monitored at i .

Each head separately calculates the attention scores and Softmax is used to normalize the scores to get the attention weight matrix M_h^W . The results of all the heads are concatenated into a matrix M_O and then output as the bit matrix Y , denoting the prediction result.

Correction of CO states. The output $RP_{t+L}(ch, i)$ is used to correct the channel occupancy state $CO_{t+L}(ch, i)$ predicted in the first-phase. $RP_{t+L}(ch, i) < \theta_i$ and $CO_{t+L}(ch, i) = 1$ imply that even though a node has moved out of the interference region of i channel ch is erroneously considered to interfere at i . In that case, $CO_{t+L}(ch, i)$ is corrected to 0. Conversely, $RP_{t+L}(ch, i) \geq \theta_i$ and $CO_{t+L}(ch, i) = 0$ represent that a node has entered the interference region of i but is incorporated in the first-phase prediction. $CO_{t+L}(ch, i)$ is therefore corrected to 1.

5 PERFORMANCE EVALUATION

For evaluation, we implemented the MiLAAP framework using PyTorch 3.11.11 on the CUDA 12.4 compute platform. We evaluated the accuracy of $SSAN_1$ and $SSAN_2$, individually—in respectively predicting the future channel occupancy map and the future received power level—and also in an integrated fashion. The latter demonstrated the improvement of the prediction accuracy of channel occupancy map once corrected via node mobility detection. Our evaluation experiments also assessed the generalizability of the framework, for different channel hopping sequence periods L .

5.1 Experimental Settings

We simulated networks with nodes distributed over a rectangular region using a uniform random distribution placement model. To simulate concurrent communication that affects the channel occupancy states for a node's interference region, all networks initiate 10 random point-to-point flows in which all routes follow the shortest path between the source and destination. Each communication node independently chooses a random channel hopping sequence with period L .

To evaluate MiLAAP for different types of node mobility in the networks, we simulated three mobility models:

- **Fixed Mobility (FM):** Each node selects a fixed velocity in $[0, 10]$ m/s and direction in $[0, 2\pi]$.
- **Random Waypoint (RWP):** Each node initially chooses a random location in a random direction $a_k \in [0, 2\pi]$ in the simulation area as the destination D_k , and then it moves towards the destination with a random velocity in $[0, 10]$ m/s. The node then assigns a new random destination D_{k+1} and a random velocity when it arrives at D_k . This is repeated until the end of the simulation.
- **Smooth Random Waypoint (SRWP):** The behavior is similar to RWP, but the assignment of the next destination D_{k+1} and velocity v_{k+1} depends on a_k and v_k . A ratio ϵ is added to further limit the minimum and maximum values in the random assignment. D_{k+1} is chosen to be a location in direction $a_{k+1} \in [a_{k+1} - 2\pi\epsilon, a_{k+1} + 2\pi\epsilon]$ and velocity $v_{k+1} \in [\max(0, (1 - \epsilon)v_{k+1}), \min(10, (1 + \epsilon)v_{k+1})]$.

We considered both regions with and without boundaries. In the former, mobile nodes stopped when they reach any boundary location.

Table 2: The prediction accuracy for $SSAN_1$ versus other sequence-to-sequence models

Model	Seen Periods	Prediction Accuracy		
		train dataset		test dataset
			seen periods	unseen periods
$SSAN_1$	7	100%	99.51%	99.29%
	5,7,9	100%	99.63%	99.31%
Standard Self-Attention	7	97.50%	69.43%	67.01%
	5,7,9	92.61%	70.79%	70.90%
LSTM	7	100%	80.05%	62.51%
	5,7,9	100%	78.17%	70.05%

We specify, for the separate phase evaluation experiments, the architecture for $SSAN_1$ and $SSAN_2$ in Tables 3 and 5, respectively, and for the integrated evaluation of MiLAAP in Table 6.

5.2 Testing First-Phase ($SSAN_1$) Prediction

Table 3: Experiment Parameters for $SSAN_1$

Symbol	Meaning	Value
N	size of training and testing graph	100
ρ	density of graph	4
r_T	transmission radius	1000m
r_I	interference radius	1000m
U	number of channels	16
X_1	shape of $SSAN_1$ input	$[0, 1]^{40 \times 16}$
Y_1	shape of $SSAN_1$ output	$[0, 1]^{40 \times 16}$
$EpNum_1$	# of training epochs for $SSAN_1$	100

We tested the ability of $SSAN_1$ to predict the future channel occupancy vectors at any given node. We first generated training data samples for various periods L of channel hopping sequences. (Within each data sample the CHS associated with all nodes had a common L). 200 data samples were included in both the training and testing datasets. We also generated two test datasets for testing generalizability: The first testing dataset includes seen periods of channel hopping sequences; i.e., these samples were not in the training dataset but their L matched that of some samples in the training dataset. The second training dataset had only unseen periods of channel hopping sequences. The prediction accuracy we evaluated is defined as the average accuracy for predicting the future channel occupancy at the node.

Table 2 shows that $SSAN_1$ achieves a prediction accuracy close to 100% in all classes of test samples. This validates the functionality of Eq. 4 for deriving the period and calculating the period offset to predict future CO vectors. We also performed an ablation study with a standard self-attention that eschewed the functionality in Eq. 4 to compare the ability to memorize seen periods. The decreased accuracy in the tests with unseen states demonstrates that the standard self-attention inadequately derives the period of channel hopping sequences to predict future CO vectors accurately. Also, a comparison test with an LSTM alternative test revealed that although the LSTM memorizes training data samples well (just as

$SSAN_1$ does), the accuracy and generalizability of its prediction of future CO vectors in the test datasets is significantly worse than that of $SSAN_1$.

5.3 Testing Second-Phase ($SSAN_2$) Prediction

Table 4: The prediction accuracy for $SSAN_2$

Mobility Model	Prediction Accuracy		
	w/ boundary	train dataset	test dataset
FM	N	100%	96.60%
	Y	100%	96.09%
RWP	N	100%	95.14%
	Y	100%	96.40%
SRWP	N	100%	98.63%
	Y	100%	97.72%

Next, we tested the prediction ability of $SSAN_2$ across the three different mobility models simulated in our dataset (FM, RWP, and SRWP mobility in networks with or without a boundary). For each network, we randomly choose a node i to continuously monitor the received power level of all active nodes within its sensing range to obtain the input data for $SSAN_2$. Recall that in the second phase, i associates the received power levels in previous slots with different nodes j in its sensing region. At each time slot t , $SSAN_2$ uses the measures of received power level from each node j in the previous 30 slots, s_{t-29}, \dots, s_t , to predict the received power level from j in the next time slot, s_{t+1} , and to infer whether j is within or outside the interference region by comparing that level with the threshold θ_i . We define the prediction accuracy of $SSAN_2$ as the percentage that node j is correctly predicted within (or outside of) i 's interference region.

Table 4 shows the prediction accuracy of $SSAN_2$ in networks with different mobility models. We further visualize the prediction results in Fig 4. In most cases, the predicted trajectories, starting from time slot 29 (after the solid blue lines), smoothly match the ground truth. We observe that mobile nodes in bounded networks yield a more complex mobility pattern compared to mobile nodes in unbounded networks. (The red and yellow flat line segments in Fig. 4c represent the case where nodes have stopped at the boundary; their received power level thus remains constant.) The added complexity however does not significantly affect the accuracy of

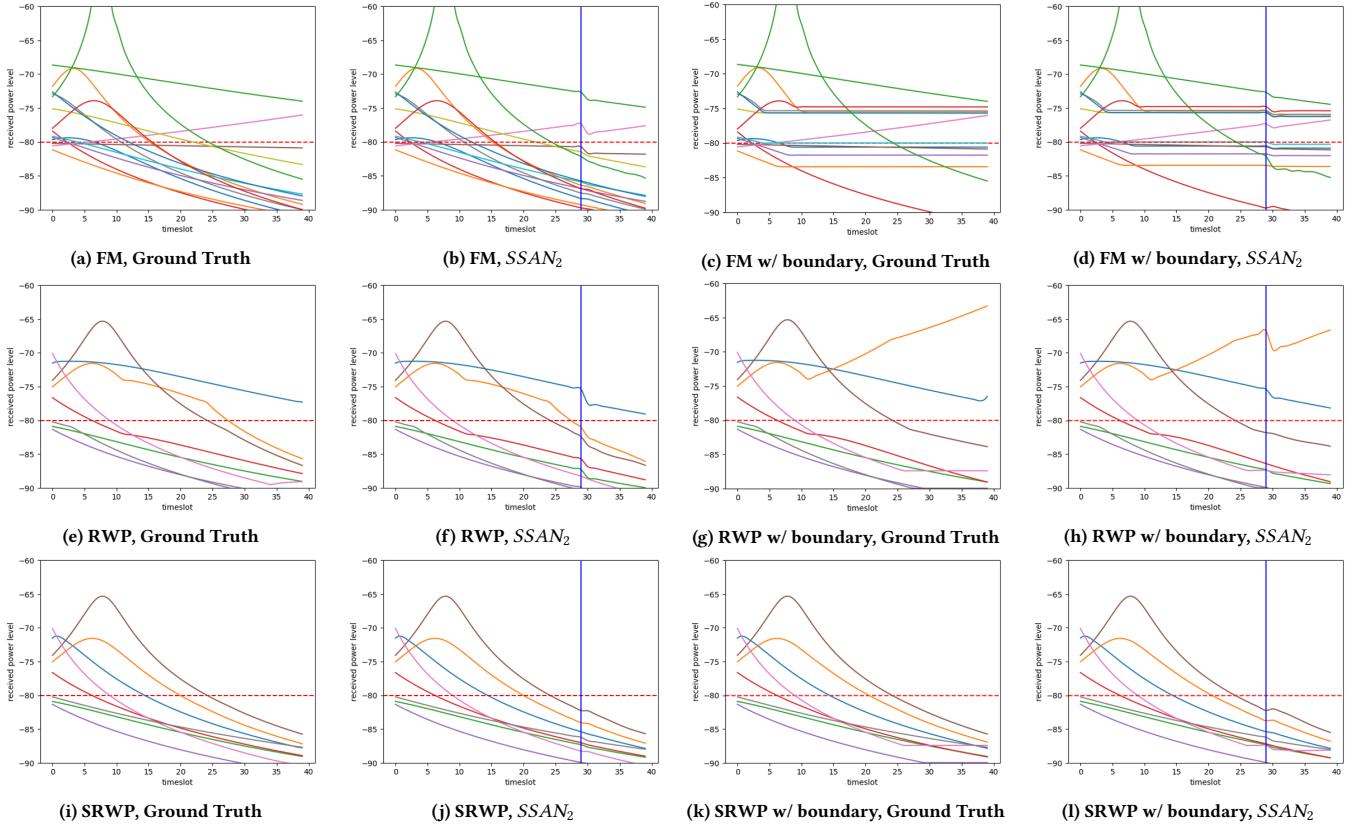


Figure 4: Examples of received power level at a node predicted by $SSAN_2$ for all mobile nodes in its sensing region, as compared with the ground truth for three mobility models. The blue solid vertical line denotes the time ($t = 29$) from which the power level prediction starts. The red dashed horizontal line denotes the threshold θ_i (in dB) for interference detection.

the prediction. Together, these results imply that a multi-head self-attention mechanism suffices to capture the temporospatial dependencies needed to predict the trajectory of mobile nodes across a diverse set of mobility models.

Table 5: Experiment Parameters for $SSAN_2$

Symbol	Meaning	Value
N	size of training and testing graph	100
ρ	density of graph	4
r_T	transmission radius	1000m
r_I	interference radius	1000m
r_S	sensing radius	1100m
ϵ	smooth ratio in SRWP	0.1
U	number of channels	16
X_2	shape of $SSAN_2$ input	\mathbb{R}^{30}
Y_2	shape of $SSAN_2$ output	\mathbb{R}
H	number of heads used in $SSAN_2$	3
$EpNum_2$	# of training epochs for $SSAN_2$	500

5.4 Integrated Testing

Table 6: Experiment Parameters in Integrated Tests

Symbol	Meaning	Value
N	size of training and testing graph	200
ρ	density of graph	4
r_T	transmission radius	1000m
r_I	interference radius	1000m
r_S	sensing radius	1100m
ϵ	smooth ratio in SRWP	0.1
U	number of channels	16
L	period of channel hopping sequences	4
X_1	shape of $SSAN_1$ input	$[0, 1]^{40 \times 16}$
Y_1	shape of $SSAN_1$ output	$[0, 1]^{40 \times 16}$
$EpNum_1$	# of training epochs for $SSAN_1$	100
X_2	shape of $SSAN_2$ input	\mathbb{R}^{10}
Y_2	shape of $SSAN_2$ output	\mathbb{R}
H	number of heads used in $SSAN_2$	4
$EpNum_2$	# of training epochs for $SSAN_2$	500

Finally, we tested the performance of the integrated first and second phases of MiLAAP. For conducting this evaluation, we generated 100 random graphs for the training and testing datasets. For each graph, 5 nodes were chosen to sample the channel occupancy state OC and the received power level RP , for a duration of 160 time slots. Each chosen node is associated with one dataset, and thus 500 datasets were collected for each mobility model.

In the integrated test, we choose 1 dataset and use its OC and RP samples to train $SSAN_1$ and $SSAN_2$, respectively. The remaining datasets are used for testing. For the prediction results of $SSAN_1$, we first show the prediction accuracy of the channel occupancy states for the test datasets in Table 7. For the portions of the state where it does not predict correctly, we further discriminate the false positive (FP) and false negative (FN) parts. Table 8 illustrates the final prediction accuracy and other metrics for the test datasets after correcting the predicted channel occupancy states according to the output of $SSAN_2$. The FP correction and the FN correction results reveal the percentage of the FP and FN OC states in Table 7 that are corrected by the output of $SSAN_2$. The correction error represents the ratio by which the accurate channel occupancy states are changed to inaccurate during correction.

Table 7 shows that the prediction of $SSAN_1$ achieves up to 93.49% accuracy in different mobility models. The FP and FN portions, respectively, indicate that about 4% and 3% of the channel occupancy states can be corrected. Table 8 shows the results for the channel occupancy states corrected using mobility detection. The prediction error (FP) of the channel occupancy states caused by the node j moving outside the interference region of node i is further corrected with a high ratio from 88.88% to 98.14%. On the other hand, the case (FN) in which node j enters i 's interference region is corrected with a ratio of at least 92.08%. Our framework only causes a negligible correction error ratio up to 0.60%. *Notably, the corrected channel occupancy results achieve an accuracy of at least 99.03% in all mobility scenarios.*

6 DISCUSSION AND CONCLUDING REMARKS

MiLAAP offers a lightweight machine learning framework for maintaining throughput efficiency in wireless networks subject to dynamics in interference and mobility, as is the case in wireless IIoT and satellite networks, by passively and locally updating local CHSes. All code and data we have developed for MiLAAP will be made publicly available along with the publication of this paper.

Our exposition of MiLAAP has associated CHSes with transmitter nodes, but they can also be readily associated in other ways: for instance, with each radio in a multi-radio node, each signal path in a MIMO radio, each receiver node, both endpoints of each link, or shared by all nodes in a path (say to achieve flow traffic pipelining along the path). While these alternative applications of MiLAAP will entail different coordination schemes between network nodes, they point to the utility of the framework in achieving diverse MAC objectives, which may include cross-layer considerations as well. They also motivate why we have deliberately not incorporated any particular form of temporal scheduling for the CHSes in Phase 3 (cf. Figure 1), explored the bootstrap or coordinated update of CHSes, or explored the role of machine learning for temporal scheduling.

Our validation of MiLAAP has shown that training from a small dataset—from only one network and with one value of L —converges quickly, has high accuracy, and generalizes to a relatively rich set of network configurations. MiLAAP training also yields accuracy in diverse mobility models, especially where mobility patterns have some structure. That said, we also expect its performance to degrade as node movements become increasingly random and frequent. Likewise, the accuracy of MiLAAP is shown to be high for relatively long-lived traffics. Dealing with approaches that work for short-lived traffics or networks where node activity is highly intermittent is a topic of future research. We also note that we did not validate MiLAAP for dynamics in external interference, but presumably it will perform well in instances where the externally induced changes to channels are persistent or have some regular structure.

REFERENCES

- [1] 2016. IEEE standard for low-rate wireless networks. *IEEE Std 802.15.4-2015 (Revision of IEEE Std 802.15.4-2011)* (2016), 1–709. <https://doi.org/10.1109/IEEESTD.2016.7460875>
- [2] 2025. Inmarsat. <https://www.inmarsat.com/>
- [3] 2025. Intelsat. <https://www.intelsat.com/>
- [4] Yaarob Al-Nidawi and Andrew H Kemp. 2015. Mobility aware framework for timeslotted channel hopping IEEE 802.15. 4e sensor networks. *IEEE Sensors Journal* 15, 12 (2015), 7112–7125.
- [5] Irmak Aykin, Marwan Krunz, and Yong Xiao. 2018. Adaptive frequency-hopping schemes for CR-based multi-link satellite networks. *International Journal of Satellite Communications and Networking* 36, 4 (2018), 315–331.
- [6] Shuqin Cao, Libing Wu, Jia Wu, Dan Wu, and Qingan Li. 2022. A spatio-temporal sequence-to-sequence network for traffic flow prediction. *Information Sciences* 610 (2022), 185–203.
- [7] Yung-Fu Chen and Anish Arora. 2022. QF-MAC: Adaptive, local channel hopping for interference avoidance in wireless meshes. *arXiv preprint arXiv:2212.08161* (2022).
- [8] Xia Cheng, Junyang Shi, and Mo Sha. 2019. Cracking the channel hopping sequences in IEEE 802.15. 4e-based industrial TSCH networks. In *Proceedings of the International Conference on Internet of Things Design and Implementation*. 130–141.
- [9] Xia Cheng, Junyang Shi, Mo Sha, and Linke Guo. 2021. Launching smart selective jamming attacks in WirelessHART networks. In *IEEE INFOCOM 2021-IEEE Conference on Computer Communications*. IEEE, 1–10.

Table 7: Performance metrics for channel occupancy prediction without correction by SSAN₂

Mobility Model		Metrics		
	w/ boundary	accuracy	false positive (FP)	false negative (FN)
FM	N	93.49%	3.62%	2.89%
	Y	93.41%	3.83%	2.76%
RWP	N	91.87%	4.40%	3.73%
	Y	91.91%	4.23%	3.86%
SRWP	N	93.32%	3.75%	2.93%
	Y	92.90%	3.90%	3.19%

Table 8: Performance metrics for channel occupancy prediction in the integrated tests

Mobility Model		Metrics			
	w/ boundary	accuracy	FP correction	FN correction	correction error
FM	N	99.67%	98.14%	97.99%	0.22%
	Y	99.49%	94.99%	99.20%	0.30%
RWP	N	99.03%	88.88%	97.77%	0.46%
	Y	99.23%	94.86%	99.66%	0.40%
SRWP	N	99.20%	91.06%	95.48%	0.49%
	Y	99.11%	96.25%	92.08%	0.60%

- [10] Hector Fenech, Alessia Tomatis, Sonya Amos, Viphakone Soumpholphakdy, and Jose Luis Serrano Merino. 2016. Eutelsat HTS systems. *International Journal of Satellite Communications and Networking* 34, 4 (2016), 503–521.
- [11] Rodrigo Teles Hermeto, Antoine Gallais, and Fabrice Theoleyre. 2017. Scheduling for IEEE802.15.4-TSCH and slow channel hopping MAC in low power industrial wireless networks: A survey. *Computer Communications* 114 (2017), 84–105.
- [12] Kyung-Gyu Lee and Seong-Jun Oh. 2020. Detection of frequency-hopping signals with deep learning. *IEEE Communications Letters* 24, 5 (2020), 1042–1046.
- [13] Younglo Lee, Jeongki Min, David K Han, and Hanseok Ko. 2019. Spectro-temporal attention-based voice activity detection. *IEEE Signal Processing Letters* 27 (2019), 131–135.
- [14] Gao Li, Jianliang Xu, Weiguo Shen, Wei Wang, Zitong Liu, and Guoru Ding. 2020. Lstm-based frequency hopping sequence prediction. In *2020 International Conference on Wireless Communications and Signal Processing (WCSP)*. IEEE, 472–477.
- [15] Qianli Ma, Shuai Tian, Jia Wei, Jiabing Wang, and Wing WY Ng. 2019. Attention-based spatio-temporal dependence learning network. *Information Sciences* 503 (2019), 92–108.
- [16] Mohamed Mohamadi, Badis Djamaa, and Mustapha Reda Senouci. 2020. Industrial internet of things over IEEE 802.15.4 TSCH networks: Design and challenges. *International Journal of Internet Technology and Secured Transactions* 10, 1-2 (2020), 61–80.
- [17] Mohamed Mohamadi and Mustapha Reda Senouci. 2018. Scheduling algorithms for IEEE 802.15.4 TSCH networks: A survey. In *International Conference on Computer Science and its Applications*. Springer, 4–13.
- [18] Marco Pettorali, Francesca Righetti, Carlo Vallati, Sajal K Das, and Giuseppe Anastasi. 2024. Mobility management in TSCH-based industrial wireless networks. *IEEE Transactions on Mobile Computing* 23, 9 (2024), 8710–8728.
- [19] D Rekha and L Pavithra. 2025. TSCH in edge IoT: A comprehensive survey of research challenges. *Transactions on Emerging Telecommunications Technologies* 36, 3 (2025), e70088.
- [20] Omid Tavallaie, Javid Taheri, and Albert Y Zomaya. 2021. Design and optimization of traffic-aware TSCH scheduling for mobile 6TiSCH networks. In *Proceedings of the International Conference on Internet-of-Things Design and Implementation*. 234–246.
- [21] Pascal Von Rickenbach, Stefan Schmid, Roger Wattenhofer, and Aaron Zollinger. 2005. A robust interference model for wireless ad-hoc networks. In *19th IEEE International Parallel and Distributed Processing Symposium*. IEEE, 8–pp.
- [22] Di Yang, Hong Li, Peng Wang, and Lihong Yuan. 2024. Multistep traffic speed prediction: A sequence-to-sequence spatio-temporal attention model. *Physica A: Statistical Mechanics and its Applications* 638 (2024), 129636.